

CIRCUIT REPRESENTATION LEARNING WITH MASKED GATE MODELING AND VERILOG-AIG ALIGNMENT

Anonymous authors

Paper under double-blind review

ABSTRACT

Understanding the structure and function of circuits is crucial for electronic design automation (EDA). Circuits can be formulated as And-Inverter graphs (AIGs), enabling efficient implementation of representation learning through graph neural networks (GNNs). Masked modeling paradigms have been proven effective in graph representation learning. However, masking augmentation to original circuits will destroy their logical equivalence, which is unsuitable for circuit representation learning. Moreover, existing masked modeling paradigms often prioritize structural information at the expense of abstract information such as circuit function. To address these limitations, we introduce MGVGA, a novel constrained masked modeling paradigm incorporating masked gate modeling (MGM) and Verilog-AIG alignment (VGA). Specifically, MGM preserves logical equivalence by masking gates in the latent space rather than in the original circuits, subsequently reconstructing the attributes of these masked gates. Meanwhile, large language models (LLMs) have demonstrated an excellent understanding of the Verilog code functionality. Building upon this capability, VGA performs masking operations on original circuits and reconstructs masked gates under the constraints of equivalent Verilog codes, enabling GNNs to learn circuit functions from LLMs. We evaluate MGVGA on various logic synthesis tasks for EDA and show the superior performance of MGVGA compared to previous state-of-the-art methods.

1 INTRODUCTION

In recent years, there has been a surge of interest in deep learning for electronic design automation (EDA), which holds great potential for achieving faster design closure and minimizing the need for extensive human supervision (Wen et al., 2022; Chen et al., 2022; Liang et al., 2023; Chen et al., 2023; Wu et al., 2024). Logic synthesis (Hachtel & Somenzi, 2005), a vital step in EDA, is a process by which an abstract specification of desired circuit behavior is turned into a design implementation for logic gates. In the field of logic synthesis, circuits can be formulated as graphs (e.g., And-Inverter graph (AIG) (Mishchenko et al., 2006)), which are well-suited for modeling element connections and topology. Consequently, GNNs (Zhang et al., 2020; Zheng et al., 2024; Chowdhury et al., 2022) have been widely used to learn the characteristics of circuits for various downstream tasks.

The effectiveness of GNNs in logic synthesis has predominantly been demonstrated in supervised settings, where task-specific labels provide the supervisory information. However, obtaining labeled data for supervised learning is costly while unlabeled circuit data is available and abundant. This discrepancy makes self-supervised learning suitable for circuit representation learning. Recent works (Wang et al., 2022; Shi et al., 2023) explored leveraging the functional aspects of circuits, such as truth tables and functional equivalence, to derive meaningful representations via the self-supervised learning paradigm. These methods excel at capturing the functional behaviors of circuits efficiently, which are crucial for many applications.

The structure of a circuit, including its layout, connectivity, gate numbers, and circuit level, plays a critical role in determining its power, performance, and area (PPA), all of which are key optimization targets of EDA. Models trained with functional targets often fall short in extracting structural details. Masked modeling paradigms, which have been successfully applied in computer vision (He et al., 2022; Bao et al., 2021), natural language processing (Kenton & Toutanova, 2019), and graph learning (Hou et al., 2023; Li et al., 2023a), offer a promising solution to learn detailed structural

054
055
056
057
058
059
060
061
062
063
064
065
066
067
068
069
070
071
072
073
074
075
076
077
078
079
080
081
082
083
084
085
086
087
088
089
090
091
092
093
094
095
096
097
098
099
100
101
102
103
104
105
106
107

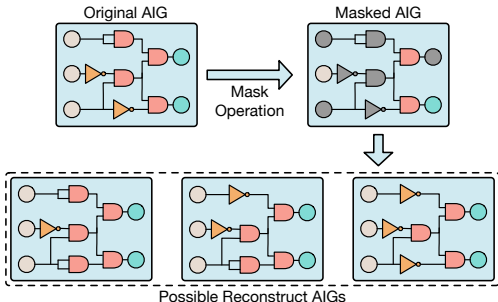


Figure 1: Possible reconstruct AIGs for masked AIG. If circuit gates are masked, there are various logic-correct solutions for reconstruction.

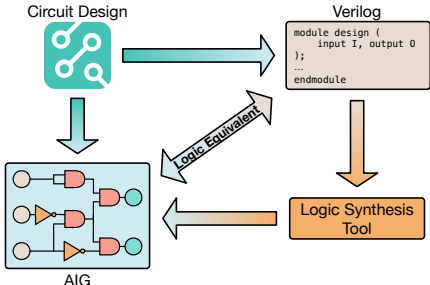


Figure 2: Logic equivalence between Verilog code and AIG. For a circuit design, AIG can be translated from Verilog code.

information. Specifically, these paradigms have proven effective in capturing the structural details of images, the syntactic and semantic structures of texts, and intricate connections in graphs. Consequently, we apply the masked modeling paradigm for circuit representation learning to extract a more fine-grained representation of the structure of circuits.

Challengingly, traditional masked graph modeling paradigm (Hou et al., 2023; Li et al., 2023a) can not be applied directly to circuit representation learning which follows strict logical equivalence. In conventional applications, such as social or molecular graphs, masking nodes typically yields a unique solution for reconstruction. However, when gates are masked in a circuit, their reconstruction will admit various solutions as illustrated in Figure 1. This is because no matter how we replace gates in the original circuits, logical correctness can still be maintained without necessarily preserving logical equivalence. Consequently, applying traditional masked modeling to circuit representation learning can not guarantee the extraction of circuit-specific features. To address this limitation, we propose a constrained masked modeling paradigm that ensures logical equivalence between the original and reconstructed circuits, thereby enabling effective circuit representation learning.

As we mentioned, abstract circuit functions are useful for EDA tasks. However, they are not explicitly represented in the structural layouts. Such functional attributes are often derived from textual descriptions in hardware description languages (HDLs), which can be processed by language models effectively. Recently, large language models (LLMs) have demonstrated remarkable performance in HDL code generation following given human instructions for circuit design (Liu et al., 2023; Pei et al., 2024; Tsai et al., 2024; Fang et al., 2024). Consequently, LLMs can serve as excellent teachers to guide GNNs in understanding circuit functions. Specifically, the AIG is logically equivalent to the corresponding behavior Verilog code for the same circuit design as illustrated in Figure 2. This equivalence allows for the alignment between Verilog codes and AIGs, facilitating GNNs’ understanding of circuit functions.

In this study, we introduce MGPGA, a constrained masked modeling paradigm incorporating Masked Gate Modeling (MGM) and Verilog-AIG Alignment (PGA) for circuit representation learning. Firstly, we introduce MGM to mask gates in the latent space instead of masking in the original circuits. This approach allows the representations of unmasked gates to serve as constraints for preserving logical equivalence when reconstructing the attributes of masked gates, as the latent representations of unmasked gates have already aggregated some features from masked gates. However, GNNs trained with MGM alone focus primarily on structural relationships within circuits, potentially overlooking function features. Considering the proficiency of LLMs in understanding Verilog code functionality, we leverage LLMs as teachers to transfer circuit function knowledge to GNNs by aligning AIGs with their logic equivalent Verilog codes. We design PGA to perform a masking operation on the original circuits and reconstruct masked gates under the constraint of corresponding Verilog codes. Although this operation will destroy the logical equivalence of the original circuits when cooperating with the traditional masked modeling strategy, we can still utilize equivalent Verilog codes as constraints to ensure the logic equivalence during the reconstruction process.

In summary, our main contributions are as follows:

- Propose masked gate modeling (MGM) for circuit representation learning, enabling GNNs to extract circuit representations with fine-grained structural information.

- Develop the Verilog-AIG alignment (VGA), which employs LLMs as teachers to guide GNNs to extract circuit representations with abstract circuit functions through equivalent AIGs and Verilog codes alignment.
- Conduct extensive evaluations and show superior performance on various logic synthesis tasks including quality of result (QoR) and logic equivalence identification compared to previous state-of-the-art (SOTA) methods.

2 RELATED WORK

AIG-Formatted Circuit Representations for Logic Synthesis. An AIG is a directed acyclic graph utilized for representing circuits (Brummayer & Biere, 2006), which is composed of AND gate, NOT gate, and terminal nodes that serve as primary inputs (PIs) and primary outputs (POs). Considering its simplicity, AIG-formatted circuits are widely used to perform circuit representation learning via GNNs. For example, Zhang et al. (2020) employs a GNN model to predict a circuit’s power consumption, and Zheng et al. (2024) proposes a customized GNN to predict the delay of circuits accurately. Besides utilizing corresponding performance metrics (power, timing, etc.) serving as labels for supervised learning, Wang et al. (2022) and Shi et al. (2023) also perform self-supervised learning for extracting general AIG-formatted circuit representation. In this study, we convert circuits to AIGs to perform general circuit representation learning via a self-supervised learning paradigm.

Masked Graph Autoencoder. Masked autoencoders (He et al., 2022; Bao et al., 2021) are based on the masked modeling learning paradigm, which involves masking a portion of the input signals and predicting the obscured content. Graph autoencoders (Hou et al., 2023; Li et al., 2023a) utilize an autoencoder architecture to encode nodes into latent representations and reconstruct the graph from these embeddings. To integrate the strengths of masked autoencoders and graph autoencoders, the masked graph autoencoder is proposed to enhance representation learning for graphs. Masked graph autoencoders randomly mask a portion of the graph nodes and then reconstruct these masked nodes using the information from the unmasked nodes and their connections. Masked graph autoencoder forces the encoder to decipher the underlying relationships within the graph, yielding robust and informative node representations. In this paper, we apply the constrained masked modeling paradigm for general circuit representation learning through the masked graph autoencoder.

LLM-based Embedding Models. LLMs, structured as decoder-only architectures, inherently face challenges in effectively encoding bidirectional context, which can impede their capacity to generate comprehensive and discriminative embeddings. Consequently, researchers apply contrastive learning for representation learning of LLMs to leverage the natural language comprehension capabilities of LLMs for embedding-related tasks (Muennighoff et al., 2024; BehnamGhader et al., 2024; Li et al., 2023b; Lee et al., 2024). This kind of strategy can help LLMs extract better representation through bidirectional attention mechanisms without hurting their own abilities. In this study, we utilize LLMs to extract Verilog codes embedding with a comprehensive understanding of circuit function, serving as constraints of the reconstruction process of VGA.

3 METHODOLOGY

Due to logical equivalence issues, traditional mask graph modeling techniques are inadequate for circuit representation learning. Additionally, GNNs have inherent limitations in extracting abstract circuit functions. To address these challenges, we propose MGPGA, a novel constrained masked modeling strategy incorporating masked gate modeling (MGM) and Verilog-AIG alignment (VGA) for enhanced circuit representation learning. AIGs have gained widespread adoption in circuit representation learning. Consequently, we convert circuits to AIGs to implement our MGPGA. In the following subsections, we will elucidate the details of MGM (Section 3.2) and VGA (Section 3.3) utilizing the AIG autoencoder. Notably, we also provide a detailed illustration of how we preserve the logic equivalence when performing MGPGA in Appendix A.1.1.

3.1 AIG AUTOENCODER

Let $\mathcal{G} = (\mathcal{V}, \mathcal{A})$ represent an AIG, where \mathcal{V} denotes the set of N nodes, $v_i \in \mathcal{V}$, categorized into four types: PI, PO, AND, and NOT gates, each labeled by $c_i \in \mathcal{C}$, $i \in \{1, 2, 3, 4\}$. The adjacency matrix

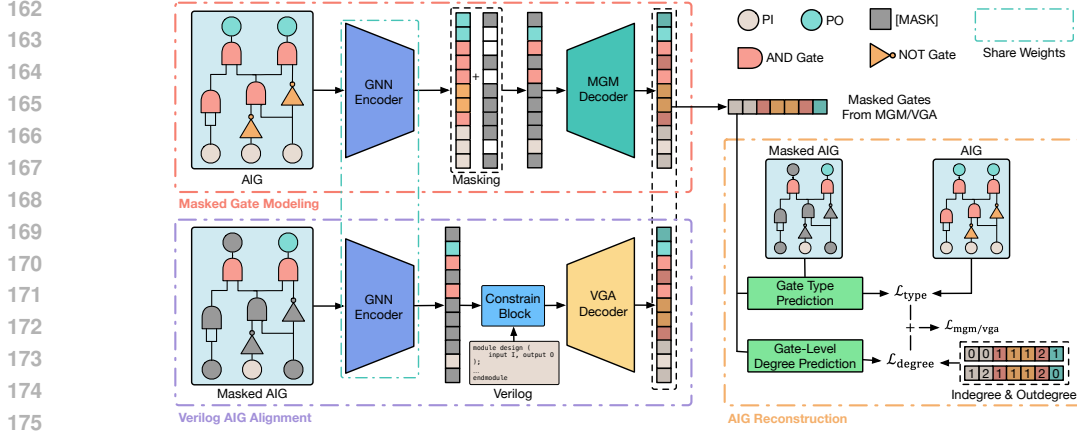


Figure 3: Overview of the MGPGA for circuit representation including masked gate modeling and Verilog-AIG alignment. For both MGM and VGA, the AIG reconstruction is implemented by gate type prediction and gate-level degree prediction from reconstructed representation.

$\mathcal{A} \in \{0, 1\}^{N \times N}$ shows the connectivity between nodes, where $\mathcal{A}_{i,j} = 1$ represents an existing edge from v_i to v_j . \mathcal{A} delineates the structure and the types of connections within \mathcal{G} .

For an AIG autoencoder, a GNN encoder, denoted by g_E , encodes \mathcal{G} into a latent space representation $\mathbf{X} \in \mathbb{R}^{N \times d}$, where d represents the dimension of this representation. The encoding process of an AIG can be formulated as:

$$\mathbf{X} = g_E(\mathcal{V}, \mathcal{A}). \quad (1)$$

Concurrently, a GNN decoder, g_D , endeavors to reconstruct the AIG \mathcal{G} from \mathbf{X} according to:

$$(\tilde{\mathbf{X}}, \mathcal{A}) = \tilde{\mathcal{G}} = g_D(\mathbf{X}, \mathcal{A}), \quad (2)$$

where $\tilde{\mathcal{G}}$ denotes the reconstructed graph, potentially encompassing both node features and structure. The primary objective of the AIG autoencoder is to optimize the encoder g_E to produce an effective representation \mathbf{X} that facilitates the accurate reconstruction of the original \mathcal{G} . Notably, following previous masked modeling paradigms (Hou et al., 2022; 2023), we do not mask the adjacent matrices \mathcal{A} during the entire process and the detailed reasons will be explained in Appendix A.1.2.

3.2 MASKED GATE MODELING

The idea of the masked autoencoder has been applied successfully to graph self-supervised learning. As an extension of denoising autoencoders, masked graph autoencoder (Hou et al., 2023; Li et al., 2023a) selectively obscure portions of the graph, such as node features or edges, through a masking operation, and learn to predict the obscured content. It has been shown that focusing solely on reconstructing masked node features as a pretext task can yield promising outcomes in graph representation learning. In traditional masked graph autoencoders, nodes are typically masked directly in the input graph before being processed through the autoencoder framework. However, this approach presents significant challenges when applied to structurally constrained graphs like AIGs, which follow strict logical rules. Utilizing a straightforward random masking technique will lead to reconstructed logic expressions that diverge from their original forms, which can not be tolerated.

To address this, we propose masked gate modeling, where the AIG is initially processed unmasked through the encoder to capture its latent representation. Rather than masking nodes at the original AIG, the masking operation is applied to the encoded representation in the latent space. During the masked modeling process, the encoder can retain the complete logical structure of the AIG before masking. This approach allows the representations of unmasked gates to serve as constraints for reconstructing the attributes of masked gates, as the latent representations of unmasked gates have already aggregated some features from masked gates.

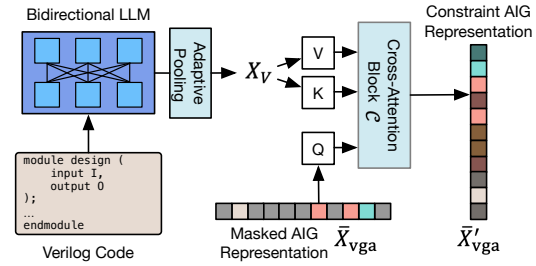


Figure 4: The constraint block for VGA.

Formally, as depicted in Figure 3, we uniformly sample a subset of gates $\mathcal{V}_{\text{mgm}} \subset \mathcal{V}$ without replacement and replace the remaining nodes with the mask token [MASK], which can be represented by a learnable vector $\mathbf{m} \in \mathbb{R}^d$. Consequently, the masked node representation $\bar{\mathbf{x}}_i \in \bar{\mathbf{X}}_{\text{mgm}}$ for each node v_i is given by:

$$\bar{\mathbf{x}}_i = \begin{cases} \mathbf{x}_i, & \text{if } v_i \in \mathcal{V}_{\text{mgm}}; \\ \mathbf{m}, & \text{if } v_i \notin \mathcal{V}_{\text{mgm}}. \end{cases} \quad (3)$$

The $\bar{\mathbf{X}}_{\text{mgm}}$ is then fed into the decoder g_D to reconstruct the \mathcal{G} following Equation (2). As illustrated in Figure 3, the decoder maintains the connectivity of each node and generates the reconstructed node representation $\tilde{\mathbf{X}}_{\text{mgm}} \in \mathbb{R}^{N \times d}$ for \mathcal{G} reconstruction (Section 3.4).

3.3 VERILOG-AIG ALIGNMENT

Although GNNs enhanced with MGM excel at extracting structural information from circuits, they often struggle to capture abstract circuit functions that are not explicitly represented in structural layouts. Meanwhile, Verilog codes contain substantial semantic information, including high-level abstract concepts and functional logic in circuit designs. Recent studies (Lu et al., 2024; Pei et al., 2024) have begun leveraging LLMs to analyze Verilog codes, highlighting the potential for distilling circuit function knowledge from LLMs to GNNs. LLMs can serve as excellent teachers, guiding GNNs in understanding circuit functions through the alignment process of equivalent Verilog codes and AIGs. Meanwhile, as illustrated in Figure 2, AIGs are translated from Verilog codes via logic synthesis tools. Consequently, there exist equivalent behavior-level Verilog codes for AIGs. Based on equivalent Verilog-AIG pairs, we can perform Verilog-AIG alignment, which conducts masking operations on original AIGs. Subsequently, the masked gates are reconstructed under the constraints of equivalent Verilog codes. This equivalence allows for the reconstruction of masked AIGs under the supervision of Verilog code, facilitating GNNs’ understanding of circuit functions.

Similar to MGM, we uniformly sample a subset of gates $\mathcal{V}_{\text{vga}} \subset \mathcal{V}$ without replacement and replace the node types of remaining nodes with c_m , which represents these nodes are masked in the original AIG. Consequently, for $v_i \in \bar{\mathcal{V}}$ of the masked AIG, the node type c_i can be defined as:

$$c_i = \begin{cases} c_i, & \text{if } v_i \in \mathcal{V}_{\text{vga}}; \\ c_m, & \text{if } v_i \notin \mathcal{V}_{\text{vga}}. \end{cases} \quad (4)$$

The masked AIG $\bar{\mathcal{G}} = (\bar{\mathcal{V}}, \mathcal{A})$ is fed into the encoder g_E to generate the encoded masked AIG representation $\bar{\mathbf{X}}_{\text{vga}}$ following Equation (1).

As mentioned earlier, the reconstruction of \mathcal{G} from $\bar{\mathbf{X}}_{\text{vga}}$ must be constrained by equivalent Verilog code to ensure strict logical equivalence. Consequently, we design a constraint block inspired by Jaegle et al. (2021) and Lee et al. (2024) as illustrated in Figure 4. Specifically, we perform adaptive pooling on token embeddings of Verilog code generated by LLMs to extract $\mathbf{X}_V \in \mathbb{R}^{M \times d_v}$, the representation of the equivalent Verilog code. We then feed the masked AIG representation $\bar{\mathbf{X}}_{\text{vga}}$ and Verilog code representation \mathbf{X}_V into a cross-attention block \mathcal{C} to perform alignment between the masked AIG and Verilog code, with $\bar{\mathbf{X}}_{\text{vga}}$ being projected to query $Q \in \mathbb{R}^{N \times d}$ and \mathbf{X}_V being projected to key $K \in \mathbb{R}^{M \times d}$ and value $V \in \mathbb{R}^{M \times d}$. Specifically, we selected $M = 16$ after carefully balancing computational cost and performance. The output of the cross attention block (Vaswani, 2017) is the constrained AIG representation $\bar{\mathbf{X}}'_{\text{vga}} \in \mathbb{R}^{N \times d}$, which can be calculated as follows:

$$\bar{\mathbf{X}}'_{\text{vga}} = \mathcal{C}(\bar{\mathbf{X}}_{\text{vga}}, \mathbf{X}_V) = \text{Softmax} \left(\frac{QK^T}{\sqrt{d}} \right) V. \quad (5)$$

After aligning the logically equivalent Verilog code and masked AIG, $\bar{\mathbf{X}}'_{\text{vga}}$ incorporates information from the abstract circuit function extracted by LLMs. Then, as illustrated in Figure 3, we obtain the reconstructed circuit representation $\tilde{\mathbf{X}}_{\text{vga}}$ from $\bar{\mathbf{X}}'_{\text{vga}}$ via g_D following Equation (2) while preserving logical equivalence. Subsequently, $\tilde{\mathbf{X}}_{\text{vga}}$ will be utilized for \mathcal{G} reconstruction, detailed in Section 3.4.

3.4 AIG RECONSTRUCTION

As illustrated in Figure 3, given the reconstructed node representations from MGM or VGA, we can predict the attributes of masked nodes. First, we predict the types of each masked node, categorizing

270 them as AND gate, NOT gate, PI, or POs. Next, we focus on the specific attributes of the nodes
 271 themselves. Specifically, AND gates have two inputs (which may be identical), while NOT gates
 272 have only one input. Moreover, PIs have no inputs, and POs have no outputs. Consequently, we pre-
 273 dict the degree of each masked node to help GNNs learn the attributes of each gate more effectively.
 274 Moreover, gate-level degree prediction aids GNNs in capturing the connectivity between gates and
 275 the overall structures of AIGs, as illustrated in Figure 3. For clarity, we unify the reconstructed node
 276 representations from MGM ($\tilde{\mathbf{X}}_{\text{mgm}} \in \mathbb{R}^{N \times d}$) and VGA ($\tilde{\mathbf{X}}_{\text{vga}} \in \mathbb{R}^{N \times d}$) into a single notation $\tilde{\mathbf{X}}$.

277 **Gate Type Prediction.** For gate type prediction, $\tilde{\mathbf{X}}$ is transformed by a mapping function $f_{\text{type}} : \mathbb{R}^d \rightarrow \mathbb{R}^C$
 278 into a categorical probability distribution over C classes. This leads to the formation
 279 of the overall probability distribution matrix $\tilde{\mathbf{Z}} \in \mathbb{R}^{N \times C}$, where each element $\tilde{Z}_{i,j}$ represents the
 280 softmax-estimated probability that node v_i belongs to class c_j . Importantly, the gate type recon-
 281 struction loss is calculated only for the N_m masked nodes:

$$283 \mathcal{L}_{\text{type}} = -\frac{1}{N_m} \sum_{\substack{i=1 \\ v_i \notin \mathcal{V}_u}}^N \sum_{j=1}^C \mathbf{Y}_{i,j} \log \tilde{Z}_{i,j}, \quad (6)$$

286 where $\mathbf{Y} \subset \{0, 1\}^{N \times C}$ and \mathbf{Y}_{ij} is a binary indicator that equals 1 if the node v_i belongs to class c_j
 287 and 0 otherwise.

288 **Gate-Level Degree Prediction.** The gate-level degree prediction involves forecasting the in-degree
 289 and out-degree of each masked gate within the AIG. Formally, given the reconstructed node repre-
 290 sentations $\tilde{\mathbf{X}}$, in-degree labels $\mathbf{D}^- \in \mathbb{R}^N$, and out-degree labels $\mathbf{D}^+ \in \mathbb{R}^N$, we utilize mean squared
 291 error as the loss function for degree regression tasks. The degree reconstruction loss, calculated only
 292 for the N_m masked nodes, is defined as:

$$294 \mathcal{L}_{\text{degree}} = \frac{1}{N_m} \sum_{\substack{i=1 \\ v_i \notin \mathcal{V}_u}}^N \left((\mathbf{D}_i^- - f_{\text{in}}(\tilde{\mathbf{X}}_i))^2 + (\mathbf{D}_i^+ - f_{\text{out}}(\tilde{\mathbf{X}}_i))^2 \right), \quad (7)$$

297 where $f_{\text{in}} : \mathbb{R}^d \rightarrow \mathbb{R}$ and $f_{\text{out}} : \mathbb{R}^d \rightarrow \mathbb{R}$ serve as mapping functions for predicting gate-level
 298 degrees. This task allows GNNs to infer the connectivity between nodes, providing insights into the
 299 interaction patterns for understanding the attributes of each gate and the organization of the circuits.
 300 As illustrated in Figure 3, the AIG reconstruction is implemented by gate type prediction and gate-
 301 level degree prediction from reconstructed representation for both MGM and VGA. Consequently,
 302 the AIG reconstruction loss for MGM and VGA can be defined as:

$$303 \mathcal{L}_{\text{mgm/vga}} = \mathcal{L}_{\text{type}} + \mathcal{L}_{\text{degree}}. \quad (8)$$

305 3.5 CONSTRAINED MASKED MODELING: MGVGA

306 Building upon the methodologies of MGM and VGA based on the AIG autoencoder, we propose
 307 a novel constrained masked modeling paradigm, MGVGA, to perform general circuit representa-
 308 tion learning. This paradigm synthesizes these strategies to develop GNNs that effectively capture
 309 diverse and intricate features of circuits. Formally, the loss function for MGVGA can be defined as:

$$311 \mathcal{L}_{\text{mgvga}} = \mathcal{L}_{\text{mgm}} + \mathcal{L}_{\text{vga}}. \quad (9)$$

312 This integration enables the GNNs to learn concurrently from fine-grained structural information and
 313 abstract circuit function features, optimizing a unified representation that facilitates a wide range of
 314 logic synthesis tasks such as classification, regression, and complex reasoning on circuits.

316 4 EXPERIMENTS

317 4.1 DATA PREPARATION

318 **AIGs Collection For MGM.** We obtain 27 circuit designs from five circuit benchmarks as our training
 319 dataset: MIT LL Labs CEP (Chetwynd et al., 2019), ITC’99 (Davidson, 1999), IWLS’05 (Al-
 320 brecht, 2005), EPFL (Amarú et al., 2015), and OpenCore (Takeda, 2008). Yosys (Wolf et al., 2013)
 321 is utilized to conduct logic synthesis, which converts source codes of circuit designs into the stan-
 322 dardized AIG format. Moreover, we prepare 1500 optimization sequences, each containing 20
 323

synthesis transformations including `rewrite`, `resub`, `refactor`, `rewrite -z`, `resub -z`, `refactor -z`, and `balance` transformations, consistent with prior works (Chowdhury et al., 2022; Zheng et al., 2024). Then sequential synthesis transformations are carried out by the logic synthesis tool ABC (Brayton & Mishchenko, 2010) and their corresponding labels are generated. Meanwhile, we also store the AIG after each synthesis transformation for AIG self-supervised learning. The resulting AIG dataset, post-technology mapping with the NanGate 45nm technology library and the “5K heavy 1k” wireload model, comprises 810000 AIGs and 40500 synthesis labels across various optimization sequences and circuit designs.

Verilog-AIG Pairs Collection For VGA. In this phase, source Verilog codes (Thakur et al., 2023; Liu et al., 2023) are selected and subjected to logic synthesis using Yosys (Wolf et al., 2013), and then they are converted into AIG format. This process yields 64826 Verilog-AIG pairs, which are utilized for VGA illustrated in Section 3.3.

AIG Preprocessing. As mentioned previously, we convert circuits to AIGs to implement our MGPGA. The node type of AIG can be categorized into four types: PI, PO, AND, and NOT gates. Given that the number of PIs and POs is typically minimal, the primary emphasis in masked modeling lies in the accurate reconstruction of AND and NOT gates. It is worth noting that the NOT gate is the only single-input logic gate. Our concern is that the model could potentially leverage the disparity in in-degrees of gates as a shortcut, thereby simplifying the reconstruction task without learning the useful circuit representations. Consequently, we introduce single-input AND gates during the training phase as illustrated in Figures 1 to 3, which have two identical inputs. The input and output of the single-input AND gate are identical, making this augmentation simply adaptable to circuits featuring various logic gates (NAND, XOR, OR, etc.). Our experiments indicate that GNNs struggle to capture degree information during the reconstruction process precisely. Consequently, we employ this augmentation method as a trick in our training process, treating it as an equivalent augmentation for AIGs to avoid overfitting and possible leakage. Notably, this augmentation is **not** utilized during the evaluation phase as shown in Figure 5.

Evaluation Dataset Collection. As for the evaluation dataset, we select 10 circuit designs external to the training dataset from opensource benchmark (Chowdhury et al., 2021; Amarú et al., 2015; OpenRISC, 2009; YosysHQ, 2020; Asanovic, 2016), the details of which are illustrated in Table 1. Additionally, we will provide more details on benchmark selection in Appendix A.2.3.

4.2 IMPLEMENTATION DETAILS

Training Process of MGPGA. For the circuit representation learning utilizing our MGPGA paradigm, we utilize DeepGCN (Li et al., 2019; 2020) as the GNN encoder and decoder. As for the LLM, we utilize `gte-Qwen2-7B-instruct` (Li et al., 2023b), trained with bidirectional attention mechanisms based on Qwen2-7B (Yang et al., 2024), which has a comprehensive understanding of abstract circuit function described in Verilog codes (Liu et al., 2023; Pei et al., 2024; Tsai et al., 2024; Fang et al., 2024). The training process employs a linear learning rate schedule with the Adam optimizer set at a learning rate of 1×10^{-3} , a weight decay of 0.01, and a batch size of 512. The model is fine-tuned for 3 epochs on $8 \times A100$ GPUs with 80G memory each. Additionally, we provide more details about the model settings in Appendix A.2.2.

Baseline Selection. As for the baseline selection, we select DeepGate2 (Shi et al., 2023) as a baseline due to its similar scope and SOTA performance in general circuit representation learning. Additionally, we provide more details of baseline selection in Appendix A.2.1.

Evaluation. To validate the efficacy of our MGPGA, we conduct evaluations across two distinct logic synthesis tasks including the Quality of Results (QoR) Prediction and Logic Equivalence Identification tasks. During the evaluation process, we utilize the GNN encoder trained with MGPGA to extract the AIG representation **without** extracting Verilog code representations. Moreover, we extract the AIG representation directly without fine-tuning DeepGate2 and MGPGA for downstream tasks. Notably, QoR prediction aims to assess the ability to extract structural information, whereas logic equivalence identification is designed to evaluate the capability of extracting abstract function information. Moreover, besides identifying logic equivalence directly, we conduct experiments on the boolean satisfiability solving (SAT) task in Appendix A.3.2. SAT solving requires rough logic equivalence checking to be strictly validated later. Additionally, we provide more details about the model settings in Appendix A.2.2.

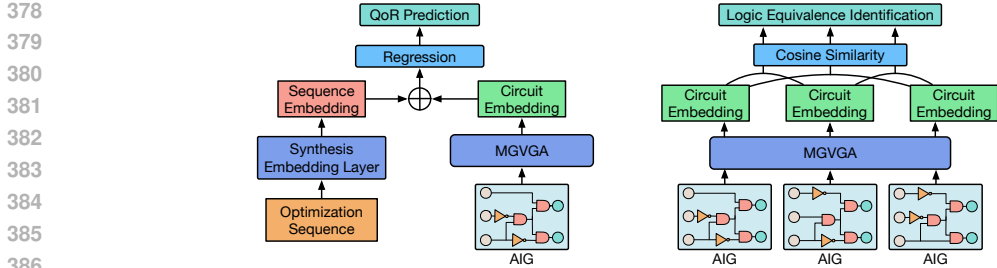


Figure 5: Application of MGVGA in QoR prediction and logic equivalence identification.

Table 1: Performance of DeepGate2 and MGVGA on QoR prediction.

Design	# PI	# PO	# Gates	DeepGate2					MGVGA (Ours)				
				NDCG@k ↑		Top-k% Commonality ↑			NDCG@k ↑		Top-k% Commonality ↑		
				k=3	k=5	k=3	k=5	k=10	k=3	k=5	k=3	k=5	k=10
bc0	21	11	2784	0.331	0.395	0.244	0.227	0.280	0.444	0.560	0.222	0.213	0.320
apex1	45	45	2661	0.645	0.643	0.222	0.333	0.413	0.706	0.716	0.311	0.400	0.513
div	128	128	101698	-0.063	0.029	0.000	0.027	0.133	-0.060	-0.060	0.000	0.013	0.093
k2	45	45	4075	-0.060	0.040	0.022	0.040	0.080	0.902	0.873	0.267	0.320	0.400
i10	257	224	3618	-0.133	-0.080	0.000	0.000	0.027	0.620	0.607	0.289	0.307	0.353
mainpla	26	49	9441	0.674	0.629	0.267	0.293	0.360	0.594	0.598	0.200	0.187	0.233
or1200_cpu	2343	2072	56570	0.498	0.485	0.178	0.267	0.407	0.617	0.613	0.222	0.253	0.367
picorv32	1631	1601	25143	0.563	0.406	0.111	0.173	0.186	0.440	0.457	0.066	0.160	0.180
Rocket	4413	4187	96507	0.578	0.543	0.111	0.186	0.300	0.557	0.607	0.355	0.413	0.467
sqrt	128	64	40920	0.304	0.153	0.000	0.027	0.080	0.577	0.401	0.000	0.040	0.080
Average				0.334	0.324	0.116	0.157	0.226	0.540	0.537	0.193	0.231	0.301

4.3 QoR PREDICTION

For QoR prediction tasks, we estimate the number of optimized gates for the circuit designs following logic synthesis optimization via ABC (Brayton & Mishchenko, 2010). As illustrated in Figure 5(a), we utilize a GNN encoder to extract circuit embeddings exclusively from AIGs. These embeddings are extracted to train the QoR prediction model with the datasets described in Section 4.1. We evaluate the performance across ten circuit designs as illustrated in Table 1, with each circuit undergoing synthesis through 1500 optimization sequences, each containing 20 steps. Notably, we detail the evaluation process and evaluation metrics of QoR prediction task in Appendix A.2.4. Specifically, we utilize two evaluation metrics including NDCG@k for k = 3, 5 and Top-k% Commonality for k = 3, 5, 10 in our experiments.

Table 1 illustrates a detailed comparison between MGVGA and DeepGate2 in QoR prediction, using the post-synthesis number of gates. MGVGA excels in NDCG@k for k = 3, 5 and achieves higher percentages in Top-k% Commonality for k = 3, 5, 10 across various designs. When considering the average performance, MGVGA notably surpasses DeepGate2 with an NDCG@3 of 0.540 compared to 0.334, and a Top-10% Commonality score of 0.301 against 0.226. This demonstrates MGVGA’s superior capability in extracting structure information of circuits, which facilitates recommending optimal optimization sequences. Collectively, these results quantitatively validate the significant advancement of MGVGA over DeepGate2 in logic circuit optimization tasks, particularly in accurately and efficiently predicting superior gate configurations to enhance overall design quality.

4.4 LOGIC EQUIVALENCE IDENTIFICATION

Each design in Table 2 undergoes optimization to generate various graph expressions while ensuring functionality equivalence. The Cone, specifying the PIs and PO constructs, also denotes functionality equivalence. To evaluate the GNNs’ ability to identify circuit function, we derive logically equivalent gates by isolating the Cone among the designs in Table 2 within AIGs using the cone command within logic synthesis tool ABC (Brayton & Mishchenko, 2010). Our dataset consists of 10000 pairs of logic gates to test the identification of logic equivalence. As illustrated in Figure 5(b), GNNs deem pairs of logic gates as equivalent if the cosine similarity between their embeddings exceeds a predefined threshold during the evaluation process. The predefined threshold is optimized based on the receiver operating characteristic (ROC) curve. In our experiments, we assess the GNNs’ performance using precision, recall, F1-score, and the area under the ROC curve (AUC).

Table 2: Performance of DeepGate2 and MGPGA on logic equivalence identification.

Design	DeepGate2				MGPGA (Ours)			
	Precision	Recall	F1-Score	AUC	Precision	Recall	F1-Score	AUC
bc0	0.199	0.930	0.327	0.813	0.274	0.715	0.396	0.817
apex1	0.133	0.680	0.223	0.601	0.273	0.710	0.394	0.826
div	0.203	0.980	0.337	0.814	0.197	0.670	0.305	0.725
k2	0.171	0.720	0.276	0.695	0.336	0.920	0.492	0.919
i10	0.414	0.940	0.575	0.918	0.699	0.950	0.805	0.985
mainpla	0.178	0.790	0.290	0.732	0.167	0.900	0.281	0.746
or1200_cpu	0.451	0.790	0.575	0.823	0.356	0.950	0.518	0.929
picorv32	0.448	0.870	0.592	0.918	0.440	0.960	0.604	0.941
Rocket	0.346	0.930	0.504	0.892	0.388	1.000	0.559	0.952
sqrt	0.189	0.740	0.302	0.721	0.199	0.720	0.312	0.770
Average	0.295	0.841	0.424	0.804	0.336	0.848	0.470	0.862

Table 3: Performance of MGPGA on QoR prediction and logic equivalence identification with different masking ratios of MGM and VGA.

Masking Ratio		QoR Prediction					Logic Equivalence Identification			
MGM	VGA	NDCG@k ↑		Top-k% Commonality ↑			Precision	Recall	F1-Score	AUC
		k=3	k=5	k=3	k=5	k=10				
0.3	0.3	0.517	0.505	0.158	0.199	0.272	0.300	0.844	0.430	0.846
0.3	0.5	0.540	0.537	0.193	0.231	0.301	0.336	0.848	0.470	0.862
0.3	0.7	0.498	0.514	0.178	0.223	0.299	0.316	0.823	0.441	0.820
0.5	0.3	0.439	0.445	0.149	0.187	0.271	0.274	0.821	0.402	0.821
0.5	0.5	0.438	0.470	0.169	0.204	0.288	0.331	0.829	0.450	0.836
0.5	0.7	0.385	0.415	0.140	0.168	0.247	0.304	0.833	0.433	0.817
0.7	0.3	0.347	0.367	0.127	0.160	0.242	0.292	0.871	0.421	0.828
0.7	0.5	0.400	0.366	0.111	0.175	0.228	0.313	0.823	0.433	0.832
0.7	0.7	0.366	0.359	0.138	0.169	0.226	0.305	0.794	0.425	0.822

As illustrated in Table 2, our proposed MGPGA has shown significant superiority over the established DeepGate2. The comprehensive analysis reveals that MGPGA outperforms DeepGate2, achieving an F1-score of 0.470 compared to 0.424, and an AUC of 0.862 versus 0.804. Moreover, we also provide more experiment results for the comparison between DeepGate3 and MGPGA using small designs in Appendix A.3.1. These results underscore the consistency of MGPGA and its superior ability to accurately determine functionally equivalent circuits, highlighting its effectiveness in extracting abstract circuit function features.

4.5 ANALYSIS OF MASKING RATIO

This section analyzes the impact of masking ratios for both MGM and VGA. Table 3 indicates that the optimal masking ratio for MGM is 0.3, while the optimal masking ratio for VGA is 0.5. At an MGM masking ratio of 0.3, the MGPGA method demonstrates notable performance. Meanwhile, there is a consistent improvement in both QoR prediction and logic equivalence identification tasks when the VGA masking ratio increases from 0.3 to 0.5.

The study reveals that higher MGM masking ratios negatively affect QoR performance, suggesting that excessive masking impedes the GNNs’ ability to learn information effectively. Specifically, excessively high masking ratios (0.5 and 0.7) significantly reduce the performance of MGPGA in the QoR prediction task, which reflects the capability in structural circuit information extraction. As for VGA, a relatively higher masking ratio (0.5) generally yields better performance for the logic equivalence identification task. An excessively high masking ratio (0.7) degrades the performance of extracting circuit structural and functional features. These findings align with our intuitive expectations. MGM directly enables GNNs to recover complete structural information from masked latent space. GNNs can not learn effective information from unmasked gates if the masking ratio is too high. In the VGA task, introducing Verilog codes as constraints for circuit restoration allows for a relatively high masking ratio, as Verilog codes contain rich circuit information.

4.6 EFFECTIVENESS OF CONSTRAINT MASKED MODELING

To assess the effectiveness of our MGM and VGA approaches, we conduct an ablation study on QoR prediction and logic equivalence identification tasks. We use the original masked modeling

Table 4: Ablation study on constraint masked modeling paradigm, including MGM and VGA.

Mask Strategy		QoR Prediction					Logic Equivalence Identification			
MGM	VGA	NDCG@ k \uparrow		Top- k % Commonality \uparrow			Precision	Recall	F1-Score	AUC
		$k=3$	$k=5$	$k=3$	$k=5$	$k=10$				
\times	\times	0.153	0.207	0.107	0.159	0.255	0.264	0.793	0.382	0.790
\checkmark	\times	0.338	0.368	0.135	0.197	0.289	0.305	0.850	0.433	0.833
\checkmark	\checkmark	0.540	0.537	0.193	0.231	0.301	0.336	0.848	0.470	0.862

Table 5: Generalization on various GNNs, including GraphSAGE and graph transformer.

GNNs	QoR Prediction					Logic Equivalence Identification			
	NDCG@ k \uparrow		Top- k % Commonality \uparrow			Precision	Recall	F1-Score	AUC
	$k=3$	$k=5$	$k=3$	$k=5$	$k=10$				
DeepGate2	0.334	0.324	0.116	0.157	0.226	0.295	0.841	0.424	0.804
GraphSAGE	0.469	0.479	0.153	0.224	0.314	0.329	0.811	0.455	0.841
Graph Transformer	0.452	0.470	0.154	0.212	0.311	0.324	0.789	0.450	0.831
DeepGCN (Ours)	0.540	0.537	0.193	0.231	0.301	0.336	0.848	0.470	0.862

strategy (Hou et al., 2023) as a baseline, employing a masking ratio of 0.3 for both the original and MGM methods, based on the optimal performance observed in Table 3.

As shown in Table 4, the original masked modeling strategy yielded poor performance in both tasks. This outcome aligns with our previous assertion that masking in the original circuits disrupts their logical equivalence, thereby preventing the method from learning effective circuit features. In contrast, both our MGM and VGA approaches demonstrated significant improvements in the two tasks, underscoring their effectiveness in enhancing GNNs’ capacity to extract fine-grained structural information and abstract functional data. Furthermore, VGA not only facilitates GNNs’ extraction of circuit function features but also enhances their ability to recognize circuit structure during the reconstruction process. This improvement occurs under the constraint of logically equivalent Verilog codes, highlighting the versatility of our VGA approach.

4.7 GENERALIZATION ON VARIOUS GNNs

To evaluate the generalization capability of our MGPGA, we perform circuit representation learning using various traditional GNNs, including GraphSAGE (Hamilton et al., 2017) and graph transformer (Shi et al., 2021). Similarly, based on the optimal performance observed in Table 3, where MGPGA achieves the best results with the MGM masking ratio of 0.3 and the VGA masking ratio of 0.5, we apply these same masking ratios to the constrained masked modeling of other GNNs.

As shown in Table 5, all GNNs trained with MGPGA exhibited significant improvements compared to the baseline DeepGate2 model. These results demonstrate the exceptional generalization ability of our proposed methods across different GNN architectures. This consistent performance enhancement across various models underscores the robustness and versatility of our MGPGA paradigm in extracting better circuit representation via circuit representation learning.

5 CONCLUSION

In conclusion, this study introduces a novel constrained mask modeling paradigm, MGPGA, for circuit representation learning. This method integrates MGM and VGA to extract fine-grained structural information and abstract functions of circuits. MGM operates by masking gates in the latent space rather than in the original circuits, subsequently reconstructing the attributes of these masked gates. This approach preserves the logical equivalence of circuits, overcoming the limitations of traditional masked gate modeling strategies. However, MGM primarily focuses on circuit structure instead of circuit function. Meanwhile, LLMs have demonstrated excellent comprehension of the Verilog code functionality. Consequently, we developed VGA, which performs masking operations on the original circuits and reconstructs them under the constraints of equivalent Verilog codes, enabling GNNs to learn circuit functions from LLMs. Our comprehensive evaluations demonstrate the superior performance of MGPGA compared to previous SOTA methods in QoR prediction and logic equivalent identification tasks. This represents a significant advancement in applying the constrained masked modeling paradigm to general circuit representation learning.

REFERENCES

- 540
541
542 Christoph Albrecht. IWLS 2005 benchmarks. *IEEE/ACM International Workshop on Logic Synthesis*, 2005.
543
- 544 Luca Amarú, Pierre-Emmanuel Gaillardon, and Giovanni De Micheli. The EPFL combinational
545 benchmark suite. In *IEEE/ACM International Workshop on Logic Synthesis*, 2015.
546
- 547 Krste others Asanovic. The Rocket Chip Generator. *EECS Department, University of California,*
548 *Berkeley, Tech. Rep. UCB/EECS-2016-17*, 2016.
- 549 Hangbo Bao, Li Dong, Songhao Piao, and Furu Wei. BEiT: BERT Pre-Training of Image Trans-
550 formers. In *International Conference on Learning Representations (ICLR)*, 2021.
551
- 552 Parishad BehnamGhader, Vaibhav Adlakha, Marius Mosbach, Dzmitry Bahdanau, Nicolas Chapa-
553 dos, and Siva Reddy. LLM2Vec: Large Language Models Are Secretly Powerful Text Encoders.
554 *arXiv preprint*, 2024.
- 555 Robert Brayton and Alan Mishchenko. ABC: An academic industrial-strength verification tool. In
556 *International Conference on Computer-Aided Verification (CAV)*, pp. 24–40, 2010.
557
- 558 Robert Brummayer and Armin Biere. Local Two-Level And-Inverter Graph Minimization without
559 Blowup. *Proc. MEMICS*, 6:32–38, 2006.
- 560 Hao Chen, Kai-Chieh Hsu, Walker J Turner, Po-Hsuan Wei, Keren Zhu, David Z Pan, and Haoxing
561 Ren. Reinforcement Learning Guided Detailed Routing for Custom Circuits. In *ACM Interna-*
562 *tional Symposium on Physical Design (ISPD)*, pp. 26–34, 2023.
563
- 564 Jingsong Chen, Jian Kuang, Guowei Zhao, Dennis J-H Huang, and Evangeline FY Young. PROS
565 2.0: A plug-in for routability optimization and routed wirelength estimation using deep learning.
566 *IEEE Transactions on Computer-Aided Design of Integrated Circuits and Systems (TCAD)*, 42
567 (1):164–177, 2022.
- 568 Brendon Chetwynd, Kevin Bush, and Kyle Ingols. Common Evaluation Platform. [https://](https://github.com/mit-ll/CEP.git)
569 github.com/mit-ll/CEP.git, 2019.
570
- 571 Animesh Basak Chowdhury, Benjamin Tan, Ramesh Karri, and Siddharth Garg. OpenABC-D: A
572 Large-Scale Dataset For Machine Learning Guided Integrated Circuit Synthesis. *arXiv preprint*,
573 2021.
- 574 Animesh Basak Chowdhury, Benjamin Tan, Ryan Carey, Tushit Jain, Ramesh Karri, and Sid-
575 dharth Garg. Bulls-Eye: Active few-shot learning guided logic synthesis. *IEEE Transactions*
576 *on Computer-Aided Design of Integrated Circuits and Systems (TCAD)*, 42(8):2580–2590, 2022.
577
- 578 Scott Davidson. Characteristics of the ITC’99 benchmark circuits. In *IEEE International Test*
579 *Synthesis Workshop (ITSW)*, 1999.
- 580 Wenji Fang, Mengming Li, Min Li, Zhiyuan Yan, Shang Liu, Hongce Zhang, and Zhiyao Xie.
581 AssertLLM: Generating and Evaluating Hardware Verification Assertions from Design Specifica-
582 tions via Multi-LLMs. *arXiv preprint*, 2024.
- 583 Winston Haaswijk, Mathias Soeken, Alan Mishchenko, and Giovanni De Micheli. Sat-based exact
584 synthesis: Encodings, topology families, and parallelism. *IEEE Transactions on Computer-Aided*
585 *Design of Integrated Circuits and Systems (TCAD)*, 2019.
586
- 587 Gary D Hachtel and Fabio Somenzi. *Logic synthesis and verification algorithms*. Springer Science
588 & Business Media, 2005.
- 589 Will Hamilton, Zhitao Ying, and Jure Leskovec. Inductive representation learning on large graphs.
590 In *Annual Conference on Neural Information Processing Systems (NIPS)*, 2017.
591
- 592 Kaiming He, Xinlei Chen, Saining Xie, Yanghao Li, Piotr Dollár, and Ross Girshick. Masked
593 Autoencoders Are Scalable Vision Learners. In *IEEE Conference on Computer Vision and Pattern*
Recognition (CVPR), pp. 16000–16009, 2022.

- 594 Zhenyu Hou, Xiao Liu, Yukuo Cen, Yuxiao Dong, Hongxia Yang, Chunjie Wang, and Jie Tang.
595 Graphmae: Self-supervised masked graph autoencoders. In *ACM SIGKDD Conference on Knowl-*
596 *edge Discovery and Data Mining (KDD)*, pp. 594–604, 2022.
- 597 Zhenyu Hou, Yufei He, Yukuo Cen, Xiao Liu, Yuxiao Dong, Evgeny Kharlamov, and Jie Tang.
598 GraphMAE2: A Decoding-Enhanced Masked Self-Supervised Graph Learner. In *ACM Web Con-*
599 *ference (WWW)*, pp. 737–746, 2023.
- 601 Andrew Jaegle, Sebastian Borgeaud, Jean-Baptiste Alayrac, Carl Doersch, Catalin Ionescu, David
602 Ding, Skanda Koppula, Daniel Zoran, Andrew Brock, Evan Shelhamer, et al. Perceiver io: A
603 general architecture for structured inputs & outputs. *arXiv preprint arXiv:2107.14795*, 2021.
- 604 Kalervo Järvelin and Jaana Kekäläinen. Cumulated gain-based evaluation of ir techniques. *ACM*
605 *Transactions on Information Systems (TOIS)*, 20(4):422–446, 2002.
- 606 Kalervo Järvelin and Jaana Kekäläinen. IR evaluation methods for retrieving highly relevant docu-
607 ments. In *ACM SIGIR Forum*, volume 51, pp. 243–250, 2017.
- 608 Jacob Devlin Ming-Wei Chang Kenton and Lee Kristina Toutanova. BERT: Pre-training of Deep
609 Bidirectional Transformers for Language Understanding. In *Annual Conference of the North*
610 *American Chapter of the Association for Computational Linguistics (NAACL)*, pp. 4171–4186,
611 2019.
- 612 Chankyu Lee, Rajarshi Roy, Mengyao Xu, Jonathan Raiman, Mohammad Shoeybi, Bryan Catan-
613 zaro, and Wei Ping. NV-Embed: Improved Techniques for Training LLMs as Generalist Embed-
614 ding Models. *arXiv preprint arXiv:2405.17428*, 2024.
- 615 Guohao Li, Matthias Muller, Ali Thabet, and Bernard Ghanem. DeepGCNs: Can GCNs go as deep
616 as CNNs? In *IEEE International Conference on Computer Vision (ICCV)*, pp. 9267–9276, 2019.
- 617 Guohao Li, Chenxin Xiong, Ali Thabet, and Bernard Ghanem. DeeperGCN: All you need to train
618 deeper GCNs. *arXiv preprint arXiv:2006.07739*, 2020.
- 619 Jintang Li, Ruofan Wu, Wangbin Sun, Liang Chen, Sheng Tian, Liang Zhu, Changhua Meng, Zibin
620 Zheng, and Weiqiang Wang. What’s Behind the Mask: Understanding Masked Graph Model-
621 ing for Graph Autoencoders. In *ACM SIGKDD Conference on Knowledge Discovery and Data*
622 *Mining (KDD)*, pp. 1268–1279, 2023a.
- 623 Zehan Li, Xin Zhang, Yanzhao Zhang, Dingkun Long, Pengjun Xie, and Meishan Zhang. Towards
624 general text embeddings with multi-stage contrastive learning. *arXiv preprint arXiv:2308.03281*,
625 2023b.
- 626 Rongjian Liang, Siddhartha Nath, Anand Rajaram, Jiang Hu, and Haoxing Ren. BufFormer: A
627 Generative ML Framework for Scalable Buffering. In *IEEE/ACM Asia and South Pacific Design*
628 *Automation Conference (ASPDAC)*, pp. 264–270, 2023.
- 629 Shang Liu, Wenji Fang, Yao Lu, Qijun Zhang, Hongce Zhang, and Zhiyao Xie. RTLCoder: Outper-
630 forming GPT-3.5 in design RTL generation with our open-source dataset and lightweight solution.
631 *arXiv preprint*, 2023.
- 632 Yao Lu, Shang Liu, Qijun Zhang, and Zhiyao Xie. RTLLM: An Open-Source Benchmark for
633 Design RTL Generation with Large Language Model. In *IEEE/ACM Asia and South Pacific*
634 *Design Automation Conference (ASPDAC)*, 2024.
- 635 Alan Mishchenko, Satrajit Chatterjee, and Robert Brayton. DAG-aware AIG rewriting a fresh look
636 at combinational logic synthesis. In *ACM/IEEE Design Automation Conference (DAC)*, pp. 532–
637 535, 2006.
- 638 Niklas Muennighoff, Hongjin Su, Liang Wang, Nan Yang, Furu Wei, Tao Yu, Amanpreet Singh, and
639 Douwe Kiela. Generative Representational Instruction Tuning. *arXiv preprint*, 2024.
- 640 OpenRISC. OpenRISC - OR1200. <https://github.com/openrisc/or1200>, 2009.
- 641
- 642
- 643
- 644
- 645
- 646
- 647

- 648 Zehua Pei, Hui-Ling Zhen, Mingxuan Yuan, Yu Huang, and Bei Yu. BetterV: Controlled Verilog
649 Generation with Discriminative Guidance. *arXiv preprint*, 2024.
- 650
- 651 Yunsheng Shi, Zhengjie Huang, Shikun Feng, Hui Zhong, Wenjin Wang, and Yu Sun. Masked label
652 prediction: Unified message passing model for semi-supervised classification. In *International
653 Joint Conference on Artificial Intelligence (IJCAI)*, 2021.
- 654 Zhengyuan Shi, Hongyang Pan, Sadaf Khan, Min Li, Yi Liu, Junhua Huang, Hui-Ling Zhen, Mingx-
655 uan Yuan, Zhufei Chu, and Qiang Xu. DeepGate2: Functionality-aware circuit representation
656 learning. In *IEEE/ACM International Conference on Computer-Aided Design (ICCAD)*, pp. 1–9,
657 2023.
- 658 Zhengyuan Shi, Ziyang Zheng, Sadaf Khan, Jianyuan Zhong, Min Li, and Qiang Xu. Deepgate3:
659 Towards scalable circuit representation learning. In *IEEE/ACM International Conference on
660 Computer-Aided Design (ICCAD)*, 2024.
- 661
- 662 Kazuyuki Takeda. OpenCores. <https://opencores.org/>, 2008.
- 663
- 664 Shailja Thakur, Baleegh Ahmad, Zhenxing Fan, Hammond Pearce, Benjamin Tan, Ramesh Karri,
665 Brendan Dolan-Gavitt, and Siddharth Garg. Benchmarking Large Language Models for Auto-
666 mated Verilog RTL Code Generation. In *IEEE/ACM Proceedings Design, Automation and Test in
667 Eurpoe (DATE)*, pp. 1–6, 2023.
- 668 Yun-Da Tsai, Mingjie Liu, and Haoxing Ren. RTLFixer: Automatically Fixing RTL Syntax Errors
669 with Large Language Models. *arXiv preprint*, 2024.
- 670
- 671 A Vaswani. Attention is all you need. In *Annual Conference on Neural Information Processing
672 Systems (NIPS)*, 2017.
- 673 Ziyi Wang, Chen Bai, Zhuolun He, Guangliang Zhang, Qiang Xu, Tsung-Yi Ho, Bei Yu, and
674 Yu Huang. Functionality Matters in Netlist Representation Learning. In *ACM/IEEE Design
675 Automation Conference (DAC)*, pp. 61–66, 2022.
- 676 Liangjian Wen, Yi Zhu, Lei Ye, Guojin Chen, Bei Yu, Jianzhuang Liu, and Chunjing Xu. Lay-
677 ouTransformer: Generating Layout Patterns with Transformer via Sequential Pattern Modeling.
678 In *IEEE/ACM International Conference on Computer-Aided Design (ICCAD)*, pp. 1–9, 2022.
- 679
- 680 Clifford Wolf, Johann Glaser, and Johannes Kepler. Yosys-a free Verilog synthesis suite. In *Austrian
681 Workshop on Microelectronics (Austrochip)*, 2013.
- 682 Haoyuan Wu, Zhuolun He, Xinyun Zhang, Xufeng Yao, Su Zheng, Haisheng Zheng, and Bei Yu.
683 ChatEDA: A Large Language Model Powered Autonomous Agent for EDA. *IEEE Transactions
684 on Computer-Aided Design of Integrated Circuits and Systems (TCAD)*, 2024.
- 685
- 686 An Yang, Baosong Yang, Binyuan Hui, Bo Zheng, Bowen Yu, Chang Zhou, Chengpeng Li,
687 Chengyuan Li, Dayiheng Liu, Fei Huang, et al. Qwen2 technical report. *arXiv preprint
688 arXiv:2407.10671*, 2024.
- 689 YosysHQ. PicoRV32 - A Size-Optimized RISC-V CPU. [https://github.com/YosysHQ/
690 picorv32](https://github.com/YosysHQ/picorv32), 2020.
- 691
- 692 Yanqing Zhang, Haoxing Ren, and Brucek Khailany. GRANNITE: Graph Neural Network Inference
693 for Transferable Power Estimation. In *ACM/IEEE Design Automation Conference (DAC)*, pp. 1–
694 6, 2020.
- 695 Haisheng Zheng, Zhuolun He, Fangzhou Liu, Zehua Pei, and Bei Yu. LSTP: A Logic Synthesis Tim-
696 ing Predictor. In *IEEE/ACM Asia and South Pacific Design Automation Conference (ASPDAC)*,
697 pp. 728–733, 2024.
- 698
- 699
- 700
- 701

A APPENDIX

A.1 MORE DETAILS OF MGVGA

A.1.1 LOGIC EQUIVALENCE PRESERVATION

In traditional masked graph modeling processes, nodes in graphs are masked directly and then reconstructed without any constraint except labels of masked nodes. However, any valid circuits can be labels during the reconstruction process for circuit representation learning. It’s hard for GNNs to learn useful features for downstream tasks in this way. Consequently, we introduce constraints during the decoding process to ensure that GNNs learn useful features related to the circuit.

In our work, “logical equivalence preservation” describes the equivalence between an AIG $\mathcal{G} = (\mathcal{V}, \mathcal{A})$ and its different representations including $X = g_E(\mathcal{V}, \mathcal{A})$ and X_V . In **MGM**, \mathcal{G} and its latent space embedding X are logically equivalent. According to $X = g_E(\mathcal{V}, \mathcal{A})$, the latent space embedding X is derived from \mathcal{G} through the GNN encoding process without masking gates(nodes). Consequently, we can say that X and \mathcal{G} comes from the same truth table. In **VGA**, \mathcal{G} and its corresponding Verilog code embedding X_V are logically equivalent. X_V is extracted via LLM according to the given Verilog code and \mathcal{G} is obtained from the Verilog code via logic synthesis tools as illustrated in Figure 2. Similarly, we can say that the truth tables of X_V and \mathcal{G} are the same.

In summary, we won’t change the original structure of AIG \mathcal{G} during the reconstruction process and the logic information is retained in X or X_V as the constraint for the decoding process.

A.1.2 UNMASKED ADJACENCY MATRIX

As we mentioned, following previous masked modeling paradigms (Hou et al., 2022; 2023), we do **not** mask the adjacent matrices \mathcal{A} during the entire process. Here are the detailed reasons.

Logical Equivalence: Our MGVGA emphasizes logical equivalence during training, ensuring that the circuit has a unique solution during reconstruction. If both \mathcal{A} and X were masked, the problem would become NP-hard due to multiple possible solutions, making it much more difficult to train the model effectively and convergently.

Computational Complexity: Reconstructing the adjacency matrix \mathcal{A} would require handling a matrix of size N^2 for N gates, which is computationally infeasible for large circuits (e.g., those with millions of gates). By not masking \mathcal{A} , we only need to reconstruct the masked gate information in X , significantly reducing computational complexity and improving the efficiency of both training and inference. Moreover, both MGM and VGA in MGVGA operate at the gate level without masking the adjacency matrix \mathcal{A} , focusing on local feature extraction. Consequently, we can utilize parallel processing techniques, distributed computing, etc., to reduce overhead in both MGM and VGA stages for high-complexity circuits.

In summary, we perform the MGVGA without masking the adjacency matrix \mathcal{A} , which is the same as previous masked graph modeling methods (Hou et al., 2022; 2023). Consequently, there are only two tasks for gate-level prediction to reconstruct masked circuits as illustrated in Section 3.4.

A.2 SPECIFIC EXPERIMENT SETTINGS

A.2.1 BASELINE SELECTION

During the baseline selection process, we acknowledged and recognized the progress made with DeepGate3 (Shi et al., 2024), the upgraded version of DeepGate2 (Shi et al., 2023). However, we encountered several challenges in our practical implementation.

Specifically, DeepGate3’s architecture is built upon DeepGate2 and incorporates transformer models, which have a quadratic time complexity during attention computation. This becomes a critical issue when dealing with large-scale datasets. Our training set includes digital circuits with up to millions of gates, leading to substantial and often unmanageable computational costs during training. During the testing phase, DeepGate3 is limited to circuits with up to thousands of gates. When attempting to infer circuits with millions of gates, the computational overhead becomes prohibitively

high. This limitation makes it impractical for our use case, where we need to handle circuits of varying sizes, including very large ones.

Consequently, we choose DeepGate2 as our baseline because it’s the best model that provides a more practical and scalable solution for the digital circuits we aim to model and optimize within the EDA toolchain. Moreover, we also provide some experiment results for the comparison between DeepGate3 and MGVGA on the small-scale designs with just thousands of gates in Appendix A.3.

A.2.2 MODEL SETTINGS

Model Size. DeepGate2 (Shi et al., 2023) has 0.64M parameters with 1 layer and DeepGate3 (Shi et al., 2024) has 8.17M parameters with transformer architecture. Meanwhile, our MGVGA has only 0.12M parameters with 7 layers. According to the experiment results, MGVGA achieved much better performance compared to DeepGate2 and DeepGate3 with fewer model parameters, which demonstrates the effectiveness of our method.

Bidirectional LLM. We utilize gte-Qwen2-7B-instruct (Li et al., 2023b) model for Verilog code representation extraction, which is based on a BERT-like encoder transformer architecture with bidirectional attention. The base model of gte-Qwen2-7B-instruct, Qwen2-7B-instruct (Yang et al., 2024), is a decoder-based model with causal attention. Qwen2-7B-instruct has been extensively trained on a diverse corpus of Verilog and demonstrates an extraordinary ability to understand and process various styles and complexities of Verilog/System Verilog code, including less standardized or non-optimized representations. Although it excels in generating text and understanding sequential dependencies, it is not well-suited for embedding tasks due to its unidirectional attention mechanism. Consequently, Li et al. (2023b) proposes GTE to transform Qwen2-7B-instruct into gte-Qwen2-7B-instruct, enabling the model to capture bidirectional context while preserving the original capabilities in understanding Verilog codes.

A.2.3 BENCHMARK SELECTION

Given the practical requirements of our application, we chose DeepGate2 as our baseline. DeepGate2 uses a portion of the design from opensource benchmarks as training data. To ensure fair and reliable testing, we excluded these designs from our test set. To further validate the reliability and practicality of our method, we have supplemented our test set with designs from different opensource benchmarks (Chowdhury et al., 2021; Amarú et al., 2015; OpenRISC, 2009; YosysHQ, 2020; Asanovic, 2016) that were not used during training. These additional test sets cover a range of graph sizes and complexities, ensuring that our evaluation is comprehensive and representative of real-world EDA tool requirements.

A.2.4 EVALUATION DETAILS OF QOR PREDICTION

For the evaluation of the QoR prediction task, we evaluate the performance across ten circuit designs as illustrated in Table 1, with each circuit undergoing synthesis through 1500 optimization sequences, each containing 20 steps. Notably, normalization is applied to $\mathbf{A} \in \mathbb{R}^{1 \times 1500}$, representing the count of optimized gates per sequence, following (Chowdhury et al., 2021). Specifically, each element \mathbf{A}_i is standardized using $\mathbf{A}_i = \frac{\bar{\mathbf{A}} - \mathbf{A}_i}{\sigma_{\mathbf{A}}}$, where $\bar{\mathbf{A}}$ and $\sigma_{\mathbf{A}}$ is the mean and the standard deviation of \mathbf{A} , respectively. For QoR prediction, we need to rank the predicted scores $\mathbf{B} \in \mathbb{R}^{1 \times 1500}$ to identify the best optimization sequence. Consequently, we utilize the Normalized Discounted Cumulative Gain (NDCG) (Järvelin & Kekäläinen, 2017; Järvelin & Kekäläinen, 2002) metric to assess the quality of the ranking algorithms for the predicted scores \mathbf{B} . The $\text{NDCG}@k$ is calculated as follows:

$$\text{NDCG}@k = \left(\sum_{i=1}^k \frac{\mathbf{A}_{\text{rank}(\mathbf{B}, i)}}{\log_2(i+1)} \right) / \left(\sum_{i=1}^k \frac{\mathbf{A}_{\text{rank}(\mathbf{A}, i)}}{\log_2(i+1)} \right), \quad (10)$$

where k represents the position considered in the ranking. Here, $\text{rank}(\mathbf{A}, i)$ and $\text{rank}(\mathbf{B}, i)$ denote the indices in \mathbf{A} and \mathbf{B} of the i -th largest elements, respectively. The $\text{NDCG}@k$ score ranges from -1 to 1, with a higher score indicating better ranking performance. A perfect ranking would achieve an $\text{NDCG}@k$ score of 1. Furthermore, we evaluate and compare the predictions on a reference set of optimization sequences with actual synthesis labels using the Top- $k\%$ Commonality metrics,

Table 6: Performance of DeepGate models and MGVGA on logic equivalence identification.

Design	# PI	# PO	# Gates	DeepGate2		DeepGate3		MGVGA (Ours)	
				F1-Score	AUC	F1-Score	AUC	F1-Score	AUC
bc0	21	11	2784	0.327	0.813	0.373	0.819	0.396	0.817
apex1	45	45	2661	0.223	0.601	0.326	0.725	0.394	0.826
k2	45	45	4075	0.276	0.695	0.345	0.834	0.492	0.919
i10	257	224	3618	0.575	0.918	0.601	0.928	0.805	0.985
mainpla	26	49	9441	0.290	0.732	0.305	0.763	0.281	0.746
Average				0.338	0.752	0.390	0.834	0.474	0.859

defined as $\frac{\text{num}(\tilde{\mathbf{A}}_k \cap \tilde{\mathbf{B}}_k)}{\text{num}(\tilde{\mathbf{A}}_k)}$, where $\tilde{\mathbf{A}}_k$ and $\tilde{\mathbf{B}}_k$ represent the top $k\%$ performing optimization sequences, actual and predicted, respectively.

A.3 EXTENDED EXPERIMENTAL RESULTS

A.3.1 LOGIC EQUIVALENCE IDENTIFICATION

As shown in Table 6, we present the performance comparison between DeepGate models (Shi et al., 2023; 2024) and MGVGA on small circuit designs considering the computation overhead. The experiment results show that MGVGA outperforms DeepGate3, achieving an average F1-score of 0.474 compared to 0.390, and an average AUC of 0.859 versus 0.834.

A.3.2 BOOLEAN SATISFIABILITY SOLVING

Boolean satisfiability (SAT) solving aims to determine whether there exists an assignment of truth values that satisfies a Boolean formula. In logic synthesis, SAT solvers are indispensable for tasks such as logic optimization, ensuring both the correctness and efficiency of circuits. Despite their critical role, SAT solving remains computationally challenging, often leading to significant runtime overhead, especially for large or complex designs. To address this challenge, several studies (Haaswijk et al., 2019; Shi et al., 2023; 2024) have proposed various methods to accelerate the SAT solving process. For instance, Exact synthesis (Haaswijk et al., 2019) enhanced SAT solving by systematically varying the number of nodes and levels in directed acyclic graph (DAG) topologies, a technique referred to as Boolean fences. A Boolean fence is a partition of nodes across multiple levels, with each level containing at least one node. By tuning these parameters, they effectively constrained the search space for the SAT solver, resulting in more efficient and predictable synthesis outcomes. Despite achieving significant speedup over SAT solvers, the solution still has room for further enhancement. Building on the work presented in (Haaswijk et al., 2019), we demonstrate how MGMVA can efficiently accelerate the SAT solving process.

Exact Synthesis generates logic circuits that guarantee logical equivalence between the resulting circuit and the target logic function, intending to find an optimal implementation based on specific criteria, such as gate count or depth.

Experiment Settings. We integrate the MGMVA into the SAT solver (Haaswijk et al., 2019) to perform exact synthesis tasks. For the training process, we apply the exact synthesis process to the EPFL (Amarú et al., 2015) and IWLS (Albrecht, 2005) benchmarks using the SAT solver (Haaswijk et al., 2019) to obtain the number of nodes and levels in the subcircuits, which are subsequently used as labels. We extract the circuit embeddings from MGVGA and feed them into MLP to perform regression tasks. As for the SAT solving process with MGVGA, we first extract several small subcircuits from the original circuits following the exact synthesis process. These subcircuits, which have a maximum of 8 inputs and a single output, are still computationally challenging due to the exponential number of Boolean functions 2^{256} resulting in large runtime overhead. Then, we can use the MGMVA to predict the number of nodes and levels required for the optimal equivalent implementation of the input subcircuit and use MGMVA to further constrain the search space of the Boolean fence, thereby accelerating the SAT solving process. Finally, to assess the efficacy of our model in accelerating SAT solving, we employ DeepGate2 (Shi et al., 2023) and DeepGate3 (Shi et al., 2024) as baselines. All experiments are conducted using the same computational resources.

Evaluation Results. Table 7 and Table 8 present a runtime comparison among the exact synthesis, DeepGate2, DeepGate3, and our MGVGA settings, with runtime measured in **seconds (s)**. We

Table 7: The comparison of SAT solving runtime (solver only).

Design	# Subcircuits	Exact Synthesis	DeepGate2		DeepGate3		MGVGA (Ours)	
			Solver	Red.	Solver	Red.	Solver	Red.
adder	27	365.19	480.72	-31.64%	464.21	-27.11%	184.19	49.56%
sqrt	38	5.55	6.65	-19.82%	6.92	-24.68%	4.77	14.05%
hyp	80	328.58	351.25	-6.90%	351.71	-7.04%	213.20	35.11%
i2c	169	267.15	62.21	76.71%	34.01	87.27%	32.98	87.65%
div	1968	4033.48	1096.21	72.83%	882.59	78.12%	844.45	79.06%
Average		999.99	399.41	18.24%	347.89	21.31%	255.92	53.09%

Table 8: The comparison of SAT solving runtime (overall).

Design	Exact Synthesis	DeepGate2			DeepGate3			MGVGA (Ours)		
		Model	Solver	Overall	Model	Solver	Overall	Model	Solver	Overall
adder	365.19	0.66	480.72	481.38	10.86	464.21	475.07	0.17	184.19	184.36
sqrt	5.55	0.65	6.65	7.30	10.91	6.92	17.83	0.24	4.77	5.01
hyp	328.58	2.13	351.25	353.38	36.01	351.71	387.72	1.32	213.20	215.84
i2c	267.15	2.60	62.21	64.81	45.95	34.01	79.96	1.06	32.98	34.04
div	4033.48	40.80	1096.21	1137.01	763.71	882.89	1646.60	17.11	844.45	861.56
Average	999.99	9.37	399.41	408.78	173.49	347.89	521.38	3.99	255.92	259.91

choose exact synthesis as our baseline setting the runtime reduction compared to the baseline setting is denoted as Red. As shown in Table 7, MGVGA achieves an average runtime reduction of 53.09% while DeepGate2 and DeepGate3 achieve an average reduction of 18.24% and 21.31% separately for SAT solving process. However, it is worth noting that the SAT solver with GNN is less effective for easier cases, as the model inference process accounts for a significant portion of the total runtime as illustrated in Table 8. In general, MGVGA exhibits significant improvement compared to DeepGate models in this task, indicating that MGVGA can capture more informative abstract functional and fine-grained structural representations for solving practical SAT solving problems.